JASA ARTICLE

Deep learning and dynamic time warping for automatic mode identification in resonant ultrasound spectroscopy

Wuyi Yang,[1,a)] Deyi Lin,[1] Shanshan Sun,[1] Liguo Tang,[1,2,3,b)] and Wenyu Luo[3,4]

[1]*Key Laboratory of Underwater Acoustic Communication and Marine Information Technology, College of Ocean and Earth Sciences, Xiamen University, Xiamen 361010, China*

[2]*Shenzhen Research Institute of Xiamen University, Shenzhen 518000, China*

[3]*State Key Laboratory of Acoustics and Marine Information, Chinese Academy of Sciences, Beijing 100190, China*

[4]*University of Chinese Academy of Sciences, Beijing 100049, China*

ABSTRACT:

For piezoelectric materials with high mechanical quality factors, resonant ultrasound spectroscopy (RUS) is a superior alternative to electric resonance methods for characterizing the elastic and piezoelectric constants. Resonant mode identification constitutes the primary challenge in RUS because mode omission and overlap cannot be avoided in the measurement of resonant ultrasound spectra, which conventionally requires the labor-intensive manual matching of experimental and simulated resonance frequencies. In this study, a combination of a deep neural network (DNN) and dynamic time warping (DTW) is proposed for automatic mode identification. The DNN efficiently maps the material constants of the piezoelectric rectangular parallelepipeds to the resonance frequencies. Although computing the resonance frequencies for training the DNN is time consuming, the trained DNN is significantly faster than the Rayleigh–Ritz method. For an experimentally measured resonance frequency sequence, the generated resonance frequency sequences using the DNN form a reference dataset. A novel DTW algorithm then performs optimal alignment between the measured and reference sequences, enabling robust mode identification through maximal similarity matching. The proposed method is validated using comprehensive simulations and experimental testing on a Fuji C-213 piezoelectric sample (Fuji Ceramics Co., Ltd., Fujinomiya, Shizuoka, Japan) at multiple temperatures. The results demonstrate comparable accuracy to manual identification methods while achieving substantial efficiency improvements. https://doi.org/10.1121/10.0042987

(Received 5 September 2025; revised 5 January 2026; accepted 18 February 2026; published online 10 March 2026)

[Editor: Julien de Rosny] Pages: 2074–2084

I. INTRODUCTION

Electromechanical devices used in ultrasonic medical equipment, nondestructive testing, and underwater engineering require the fabrication of piezoelectric materials (PMs).[1] The elastic, piezoelectric, and dielectric constants of such PMs must first be characterized, which is fundamental for designing piezoelectric resonators, transducers, and numerous devices.[2,3]

The ultrasonic pulse-echo method is often combined with the electric resonance method to determine the full matrix constants of piezoelectric crystals.[4] However, the material constants obtained using these methods often lack self-consistency, because multiple samples with significantly different geometries must be used.[5,6] Comparatively, resonant ultrasound spectroscopy (RUS) can determine the elastic and piezoelectric constants (EPCs) from a single sample, eliminating inconsistencies arising from sample-to-sample variations.[6]

RUS fundamentally relies on a mapping relationship between resonance frequencies and material constants for samples of known dimensions. When measuring the sample dimensions, inversion algorithms are used to estimate the material constants from the measured resonance frequencies.[7] This backward problem is central to the RUS methodology and is conventionally addressed using nonlinear least squares (NLS) optimization, typically implemented through the Levenberg–Marquardt algorithm.[7] Iterative NLS-based RUS inversion requires repeated solving of the forward problem, which computes the resonance frequencies from the material constants. Finite element analysis (FEA) and Rayleigh–Ritz methods are common forward solvers for piezoelectric samples.[8–10]

To realize a reliable RUS inversion, sufficient resonance modes must be successfully identified.[11] The peak frequencies in the measured resonant ultrasound spectra of a piezoelectric sample are the resonance frequencies, that is, the vibration frequencies corresponding to the resonance modes. In RUS, resonance mode identification is the most challenging task because mode omission and overlap cannot be avoided during the measurement of resonant ultrasound spectra. To conduct RUS inversion, the correct sequence of resonance frequencies must first be determined. Therefore, omitted and overlapping modes must be determined. Generally, the number of identified resonance modes should

[a)]Email: wyyang@xmu.edu.cn
[b)]Email: liguotang@xmu.edu.cn

https://doi.org/10.1121/10.0042987

be optimally 8–10 times greater than the number of material constants to be determined. The greater the number of resonance modes to be identified, the wider the required frequency range for obtaining the resonant ultrasound spectra. However, as the frequency increases, the resonance modes become more densely distributed, making mode omission and overlapping inevitable, which consequently increases the difficulty of mode identification.

Mode identification requires substantial manual intervention. This involves matching the measured resonance frequencies with the calculated reference resonance frequencies based on the estimated EPCs of the PMs.[12] Successful mode identification fundamentally relies on identifying reference resonance frequencies that closely correspond to the measured frequencies. When significant discrepancies occur between the measured and reference resonance frequencies, it becomes necessary to adjust the estimated EPCs and recalculate the reference resonance frequencies for mode identification. This procedure is extremely time consuming and inherently subjective, often leading to failed mode identification attempts.

With recent advances in deep learning technology, the integration of RUS with deep learning has gained increasing attention. As a pivotal branch of machine learning, deep learning constructs models based on artificial neural networks, thereby enabling automatic feature extraction and complex task processing through nonlinear transformations. Remarkable breakthroughs have been achieved across multiple domains.[13–16] Deep learning has significantly affected the development of mechanics and acoustics.[17,18] In the mechanical or acoustic domains, traditional methods establish mapping relationships between measurement results and material properties through complex physical modeling. Deep learning offers novel solutions to such problems as neural network models are constructed to establish mappings between input parameters and output characteristics, substantially reducing computational costs while enhancing efficiency.[19–21] Yang *et al.*[22] and Yang *et al.*[23] employed deep neural networks (DNNs) to solve RUS backward problems and efficiently characterize the EPCs of PMs. Liu *et al.*[24] used resonance frequencies, differentials of resonance frequencies, or resonance frequency feature maps as inputs to neural networks to invert elastic constants. In addition, Fukuda *et al.*[25] transformed resonance frequencies into multi-channel two-dimensional (2D) feature maps by utilizing a convolutional neural network (CNN) to estimate the material constants. Moreover, Wang *et al.*[26] designed a CNN that utilizes the real components of resonant spectra and mass density as inputs to predict the elastic constants for low-Q materials. These approaches leverage DNNs for nonlinear regression from resonance frequencies to material constants, which markedly improves inversion efficiency.

Dynamic time warping (DTW)[27,28] can determine the optimal element correspondence between two sequences of different lengths and evaluate the similarity between the two sequences. Therefore, DTW may also be used for RUS mode identification. The resonance frequencies of a digital piezoelectric sample constitute a frequency sequence. A collection of these sequences, which is generated by randomly changing the material constants, forms a reference dataset for mode identification. DTW enables the identification of the reference sequence that most closely matches the measured resonance frequency sequence, thereby facilitating mode identification. However, the use of DTW for RUS mode identification has not yet been investigated.

In this study, deep learning is combined with DTW to perform automatic mode identification in RUS. A DNN for the RUS forward problem is proposed for modeling the relationship between the material and geometrical constants $\{c^{\mathrm{E}}, e, \varepsilon^{S}, \rho, w, h, l\}$ and the resonance frequencies of piezoelectric rectangular parallelepipeds, where $c^{\mathrm{E}}, e, \varepsilon^{S}$, and ρ denote the elastic stiffness constants, piezoelectric stress constants, free dielectric constants, and density, respectively, and w, h, and l denote the width, height, and length of the rectangular parallelepiped sample, respectively. Although computing the resonance frequencies for training the DNN is time consuming, the trained DNN can predict the resonance frequencies of the piezoelectric samples significantly faster than the Rayleigh–Ritz or FEA methods.

For a test piezoelectric sample, the reference resonance frequency sequence dataset for mode identification is generated using the trained DNN with a high efficiency. The dimensions, densities, and dielectric constants of the test sample can be directly measured. Therefore, during the generation of the reference dataset, the dimensions, densities, and dielectric constants of the reference digital piezoelectric samples are set to be the same as those of the test sample. For the resonance frequency sequence of the test sample, a novel DTW algorithm performs optimal alignment against this dataset through maximal similarity matching. Comprehensive simulations and experiments on a Fuji C-213 lead zirconate titanate (PZT) ceramic sample at multiple temperatures are performed to validate the proposed method. The measured resonance frequencies are automatically identified and the EPCs of the sample are determined using the trained DNN for the RUS backward problem. The combination of DNN and DTW is valuable because such characterization requires a large number of repeated implementations. For example, the providers of commercial PMs must characterize products obtained from different batches. Therefore, it is worthwhile to dedicate a large amount of time to generate digital samples for training the DNN as it will be reused many times. However, the method is not suitable for characterizing new PMs under development because the characterization of those materials does not require multiple repetitions. Therefore, the generation of numerous digital samples for training the DNN in this case is not worthwhile.

II. THEORY AND ALGORITHMS

A. RUS

RUS comprises forward and backward problems.[29] The forward problem computes the piezoelectric resonance frequencies based on the EPCs, dielectric constants, and

dimensions of the piezoelectric samples. The forward problem can be solved using the Rayleigh–Ritz method to derive the following eigenvalue problem:

$$(\Pi + \Theta\Xi^{-1}\Theta^{\mathrm{T}})\mathbf{A} = \rho\omega^2\mathbf{A}, \tag{1}$$

where Π, Θ, and Ξ are mechanical, piezoelectric, and electric matrices, respectively; $\mathbf{A}$ is the eigenvector; and ρ and ω are the density and angular frequency, respectively. The displacement u_i and electric potential ϕ of a piezoelectric body can be approximated by the sum of the linear combination of orthogonal basis functions, i.e.,

$$u_i = \sum_{p=1}^{N} a_p^{(i)} v_p \quad (i = 1, 2, 3) \tag{2}$$

and

$$\phi = \sum_{r=1}^{N} b_r \psi_r, \tag{3}$$

where $\{v_p\}$ and $\{\psi_r\}$ are orthogonal basis functions, such as Legendre functions, and $\{a_p^{(i)}\}$ and $\{b_r\}$ are coefficients. The parameter N in Eqs. (2) and (3) controls the numerical accuracy when solving Eq. (1) for the resonance frequencies. Higher N values yield greater precision at the expense of computational efficiency.

Given the resonance frequencies measured from a piezoelectric sample by the RUS system, the backward procedure estimates the EPCs, resulting in computed resonance frequencies that closely match the measured resonance frequencies.[29] The RUS backward problem can be realized by solving the NLS problem and minimizing the following function:

$$F = \frac{1}{2}\sum_{i=1}^{K} w_i \left[f_{\mathrm{cal}}^{(i)} - f_{\mathrm{meas}}^{(i)}\right]^2, \tag{4}$$

where w_i is the weighting factor and $f_{cal}^{(i)}$ and $f_{meas}^{(i)}$ are the ith measured and calculated resonance frequencies of the sample, respectively. The NLS methods, such as the Levenberg–Marquardt (LM) method, are often used to solve this problem.

During the RUS inversion procedure, the computation of the ultrasonic resonance frequencies must be repeated several dozen or even hundreds of times; therefore, the procedure usually takes tens of minutes or even several hours.[22] Thus, to improve the efficiency of RUS inversion, DNNs[22–26] have been proposed to characterize the EPCs of PMs, which are more efficient than NLS methods.

B. DNN for RUS forward problem

Mode identification involves matching the measured resonance frequencies with the calculated reference resonance frequencies based on the estimated EPCs of the PMs. Successful automatic mode identification fundamentally relies on calculating many reference resonance frequency sequences and identifying the reference resonance frequency sequence that is most similar to the measured resonance frequency sequence. However, it is time consuming to compute the reference resonance frequency sequences using the Rayleigh–Ritz method. Using this method on a desktop system [Intel® Core™ i9-10900K central processing unit (CPU) @ 3.70 GHz (Intel Corporation, Santa Clara, CA), 32.0 GB random access memory (RAM)], resonance frequency calculations for piezoelectric samples averaged 1.6 and 6.1 s under parameter configurations of $N = 16$ and $N = 20$, respectively.[26] Thus, to improve the efficiency of mode identification, the computation of the resonance frequencies must be performed with high efficiency.

1. DNN structure

In feedforward neural networks, information propagates unidirectionally—from the input layer, through one or more hidden layers, to the output layer—with no cycles or feedback loops involved. Each layer acts as a transformation function, mapping input data into a new feature representation. By stacking multiple such layers, the network progressively extracts higher-level features from the input and approximates the target function. The proposed DNN structure (Fig. 1) is a type of feedforward neural network. The first layer of the DNN structure is the normalization layer, the final layer is the scaling and shifting layer, and the intervening layers are fully connected. Specifically, for each layer from the third to the penultimate layer, the output of the previous layer and that of the first layer are concatenated as the input for that layer. The normalization layer normalizes the input data such that they exhibit zero mean and unit variance, which can help improve the stability and convergence speed of the model. The final layer scales and shifts the output from the penultimate layer, improving the performance and convergence speed of the model.

The input of the network is $\mathbf{x} = [x_1, \ldots, x_N]^{\mathrm{T}} \in \mathbf{R}^{N\times 1}$. The network output is formulated as follows:

$$\tilde{\mathbf{y}} = [\tilde{y}_1, \ldots, \tilde{y}_M]^{\mathrm{T}} = G(\mathbf{x}; \theta), \tag{5}$$

where $\mathrm{G}(\cdot; \theta)$ denotes the mapping function of the network, $\tilde{y}_i (i = 1, \ldots, M)$ is the ith neuron of the network output, M is the number of the neurons in the output layer, and θ contains the network parameters with the network. The depth of the network is K. The output of the kth layer is expressed as follows:

$$\tilde{\mathbf{x}}^{(k)} = G^{(k)}\left(\mathbf{x}^{(k)}; \theta_k\right), \tag{6}$$

where $G^{(k)}(\cdot; \theta_k)$ denotes the mapping function of the kth layer, $\mathbf{x}^{(k)}$ is the input of the kth layer, $\tilde{\mathbf{x}}^{(k)}$ is the output of the kth layer, and θ_k contains the network parameters with the kth layer.

The first layer $G^{(1)}(\mathbf{x}; \theta_1)$ is the parameter normalization layer obtained through sample statistics. For each dimension of the input $\mathbf{x}$, the first layer normalizes each

https://doi.org/10.1121/10.0042987

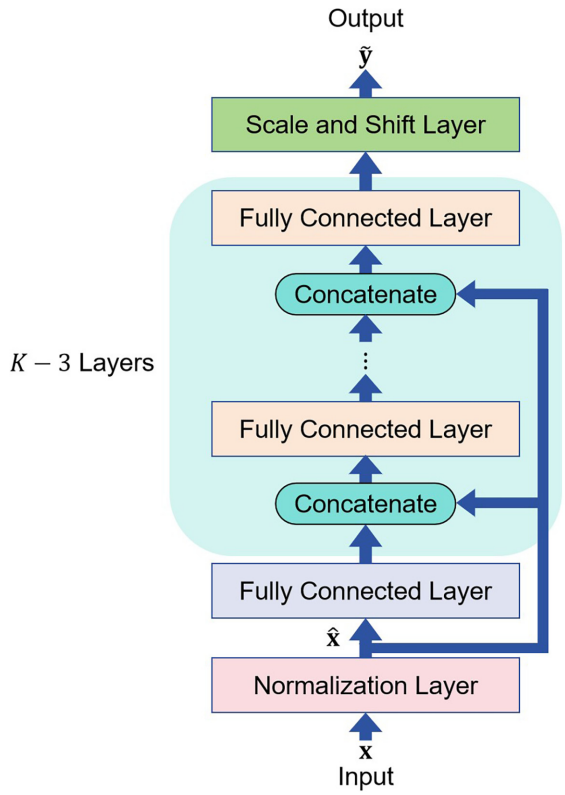

FIG. 1. DNN structure with K layers.

dimension independently such that it exhibits zero mean and unit variance as follows:

$$\hat{x}_i = \frac{x_i - \mathrm{E}[x_i]}{\sqrt{\mathrm{Var}[x_i]}} \quad (i = 1, \ldots, N), \tag{7}$$

where the expectation $\mathrm{E}[x_i]$ and variance $\mathrm{Var}[x_i]$ can be computed over the training dataset. The output of the first layer is $\tilde{\mathbf{x}}^{(1)} = \hat{\mathbf{x}} = [\hat{x}_1, \ldots, \hat{x}_N]^{\mathrm{T}}$.

Layers 2 to $K-1$ are fully connected layers, and $n^{(k)}$ is the number of neurons in the kth layer. $G^{(k)}(\mathbf{x}^{(k)}; \theta_k)$ can be written as follows:

$$\tilde{\mathbf{x}}^{(k)} = G^{(k)}\left(\mathbf{x}^{(k)}; \theta_k\right) = \sigma\left(\mathbf{W}^{(k)}\mathbf{x}^{(k)} + \mathbf{b}^{(k)}\right), \tag{8}$$

where $\mathbf{W}^{(k)} \in \mathbf{R}^{n^{(k)} \times n^{(k-1)}}$ is the weight vector, $\mathbf{b}^{(k)} \in \mathbf{R}^{n^{(k)} \times 1}$ is the bias, $\theta_k = \left\{\mathbf{W}^{(k)}, \mathbf{b}^{(k)}\right\}$, and $\sigma(\cdot)$ is the activation function, which is applied to each element of the input vector independently. As shown in Fig. 1, for the second layer, the input is $\mathbf{x}^{(2)} = \tilde{\mathbf{x}}^{(1)} = \hat{\mathbf{x}}$, and for layers 3 to $K-1$, the input is $\mathbf{x}^{(j)} = [\tilde{\mathbf{x}}^{(j)^{\mathrm{T}}}, \hat{\mathbf{x}}^{\mathrm{T}}]^{\mathrm{T}}$. The activation function is applied to layers 2 to $K-2$, and the activation function is not applied to the $(K-1)$th layer.

The final layer of the network is the scale-and-shift layer obtained via sample statistics. That is, for each element of the input vector

$$\mathbf{x}^{(K)} = \tilde{\mathbf{x}}^{(K-1)} = [x_1^{(K)}, \ldots, x_N^{(K)}]^{\mathrm{T}}, \tag{9}$$

the final layer scales and shifts each element independently by

$$\tilde{y}_i = \sqrt{\mathrm{Var}[y_i]}\, x_i^{(K)} + \mathrm{E}[y_i] \quad (i = 1, \ldots, M), \tag{10}$$

where y_i is the expected output of the ith neuron in the last layer, and the expectation $\mathrm{E}[y_i]$ and variance $\mathrm{Var}[y_i]$ can be estimated over the training dataset.

Based on the DNN structure illustrated in Fig. 1, various DNNs with different numbers of neurons and layers were generated. These DNNs have the same first and final layers. In the following discussion, $\mathrm{D}\{n^{(2)}, \ldots, n^{(K-1)}\}$ is used to represent a DNN comprising K layers: the first layer is the parameter normalization layer; the kth layer is a fully connected layer with $n^{(k)}$ neurons, where $k = 2, \ldots, K-1$; and the final layer is the scale-and-shift layer. The number of network parameters in the DNN is $\sum_{k=2}^{K-1}(n^{(k-1)} + N + 1) \times n^{(k)}$ with $n^{(1)} = 0$ and $n^{(K-1)} = M$.

The training of a DNN can be considered as a solution to the following optimization problem:

$$F = \min_{\theta} \|\mathbf{y} - G(\mathbf{x}; \theta)\|_2^2, \tag{11}$$

where $\|\cdot\|_2$ denotes the Lebesgue 2-norm, and $\mathbf{y} = [y_1, y_2, \ldots, y_M]^{\mathrm{T}}$ is the expected output of the DNN. The DNN can be trained using the backpropagation (BP) method.[30]

2. RUS forward-problem DNN

Using a DNN to model the relationship between the material constants and resonance frequencies of the piezoelectric rectangular parallelepipeds, the input of the network is the material-constant vector, while the output of the network is the predicted ultrasonic resonance frequency vector. Given the material-constant vector $\mathbf{x}$ of a piezoelectric sample, the expected output of the DNN is the ultrasonic resonance frequency vector $\mathbf{f} = [f_1, f_2, \ldots, f_M]^{\mathrm{T}}$, where $f_1, f_2, \ldots, f_M$ are M resonance frequencies of this piezoelectric sample calculated using the Rayleigh–Ritz method. Holland and EerNisse[8] derived the general theory of Rayleigh–Ritz method for piezoelectric bodies. Subsequently, Ohno numerically studied the resonance frequencies of rectangular piezoelectric parallelepipeds based on their theoretical results.[9]

For piezoelectric crystals with 3 m symmetry, the input $\mathbf{x}$ of the network corresponds to the material-constant vector, which is formulated as follows:

$$\begin{aligned}\mathbf{x} = [&c_{11}^{\mathrm{E}}, c_{12}^{\mathrm{E}}, c_{13}^{\mathrm{E}}, c_{14}^{\mathrm{E}}, c_{33}^{\mathrm{E}}, c_{44}^{\mathrm{E}}, e_{15}, e_{22}, e_{31},\\ &e_{33}, \varepsilon_{11}^{\mathrm{S}}, \varepsilon_{33}^{\mathrm{S}}, \rho, w, h, l]^{\mathrm{T}} \in \mathbf{R}^{16\times 1},\end{aligned} \tag{12}$$

where c_{11}^{E}, c_{12}^{E}, c_{13}^{E}, c_{14}^{E}, c_{33}^{E}, and c_{44}^{E} are the elastic stiffness constants, e_{15}, e_{22}, e_{31}, and e_{33} are the piezoelectric stress constants, $\varepsilon_{11}^{\mathrm{S}}$ and $\varepsilon_{33}^{\mathrm{S}}$ are the dielectric constants, ρ is the density, and w, h, and l are the width, height, and length of the piezoelectric sample, respectively. The network output is formulated as follows:

$$\tilde{\mathbf{f}} = [\tilde{f}_1, \ldots, \tilde{f}_M]^{\mathrm{T}} = \mathrm{G}(\mathbf{x}; \theta), \tag{13}$$

where $\tilde{f}_i\,(i=1,\ldots,M)$ is the ith predicted resonance frequency.

The final layer of the network is the scale-and-shift layer, which is derived from the sample statistics. For each input element of the final scale-and-shift layer, the final layer scales and shifts each element independently as follows:

$$\tilde{f}_i = \sqrt{\mathrm{Var}[f_i]}\,x_i^{(K)} + \mathrm{E}[f_i]\;(i=1,\ldots,M), \tag{14}$$

where $x_i^{(K)}$ is the ith element of the input vector of the final layer, and the expectation $\mathrm{E}[f_i]$ and variance $\mathrm{Var}[f_i]$ are computed over the training dataset. Usually, the number of resonance frequencies is much greater than the number of material parameters, so the length of the network output vector is much greater than the length of the input vector, i.e., $M \gg N$.

To train the DNN, digital piezoelectric samples can be randomly generated with diverse EPCs, clamped dielectric constants, density, and dimensions. The ultrasonic resonance frequencies of these digital piezoelectric samples can be calculated using the Rayleigh–Ritz method. Using the trained DNN, the reference resonance frequency sequences for mode identification can be calculated more efficiently than when using the traditional Rayleigh–Ritz method.

C. DTW for mode identification

1. DTW

The optimal element correspondence between two sequences of different lengths can be determined by the DTW algorithm.[27,28] Let us suppose that a warping path between two sequences $X=(x_1,x_2,\ldots,x_N)$ and $Y=(y_1,y_2,\ldots,y_M)$ is represented by the sequence $P=(p_1,p_2,\ldots,p_L)$, where $p_l=(n_l,m_l)$, $n_l\in[1:N]$, $m_l\in[1:M]$, and $1\le l\le L$. P satisfies the boundary conditions $p_1=(1,1)$ and $p_L=(N,M)$. The monotonicity condition and step size condition are $p_l-p_{l-1}\in\{(1,0),(0,1),(1,1)\}$ for $2\le l\le L$. The cost of the warping path P is defined as $c_P(X,Y)=\sum_{l=1}^{L}c(x_{n_l},y_{m_l})$, where $c(x_{n_l},y_{m_l})$ is the distance between the two elements. Because of the existence of many different element correspondences between X and Y, several warping paths exist. The optimal warping path P^* has the lowest total cost among all possible warping paths. The DTW distance $\mathrm{DTW}(X,Y)$ between X and Y is defined as the total cost of P^*:

$$\begin{aligned}\mathrm{DTW}(X,Y) &= c_{P^*}(X,Y)\\ &= \min\{c_P(X,Y)|P \text{ is an } (N,M)\\ &\quad -\text{warping path}\}.\end{aligned} \tag{15}$$

2. Subsequence DTW for mode identification

The measured resonance frequency sequence is $F^{mea}=(f_1^{mea},f_2^{mea},\ldots,f_N^{mea})$ with length N, and the calculated resonance frequency sequence is $F^{cal}=(f_1^{cal},f_2^{cal},\ldots,f_M^{cal})$ with length M. Here, $M\ge N$ due to the inevitable omission and aliasing of resonance modes in the ultrasonic resonance spectrum. Because the omission and aliasing of resonance modes in the measured resonance frequencies are inevitable, the boundary and step size conditions of the classical DTW algorithm cannot be satisfied, rendering this algorithm inapplicable to the mode identification of measured resonance frequencies.

A subsequence of F^{cal} is defined as $F^{cal}(a:b)=(f_a^{cal},f_{a+1}^{cal},\ldots,f_b^{cal})$. For mode identification, it is necessary to determine the optimal subsequence $F^{cal}(a^*:b^*)$ in F^{cal} to match F^{mea},

$$(a^*,b^*)=\underset{(a,b):1\le a<b\le M}{\mathrm{argmin}}\left(\mathrm{DTW}\left(F^{mea},F^{cal}(a:b)\right)\right). \tag{16}$$

Because two adjacent resonance frequencies in F^{mea} may correspond to two spaced resonance frequencies in F^{cal}, the step size condition of the warping path is set as $p_l-p_{l-1}\in\{(0,1),(1),\ldots,(1,T)\}$ for $2\le l\le L$, where T is the skip threshold. The distance between F^{mea} and F^{cal} is defined as

$$D\left(F^{mea},F^{cal}\right)=\mathrm{DTW}\left(F^{mea},F^{cal}(a^*:b^*)\right). \tag{17}$$

Next, we define an $N\times M$ accumulated cost matrix D, and set

$$D(n,m)=\mathrm{DTW}\left(F^{mea}(1:n),F^{cal}(a':m)\right), \tag{18}$$

where

$$a'=\underset{1\le a\le m}{\mathrm{argmin}}\left(\mathrm{DTW}\left(F^{mea}(1:n),F^{cal}(a:m)\right)\right). \tag{19}$$

Here, we obtain $b^*=\mathrm{argmin}_{1\le b\le M}D(N,b)$, $D(N,b^*)=\mathrm{DTW}(F^{mea},F^{cal}(a^*:b^*))$ and $a^*=\mathrm{argmin}_{1\le a\le b^*}(\mathrm{DTW}(F^{mea},F^{cal}(a:b^*)))$.

Theorem 1. The accumulated cost matrix D satisfies the following identities: $D(1,m)=c(f_1^{mea},f_m^{cal})$, for $m\in[1:M]$, $D(n,m)=\infty$ for $m<n$ and $1<m\le M$, and

$$\begin{aligned}D(n,m)=\min\{&D(n,m-1),D(n-1,m-1),\ldots,\\ &D(n-1,m-T)\}+c\left(f_n^{mea},f_m^{cal}\right)\end{aligned} \tag{20}$$

for $n\le m\le N$ and $1<m\le M$.

Proof. Let $n=1$ and $m\in[1:M]$. Then, $m=\mathrm{argmin}_{1\le a\le m}(\mathrm{DTW}(F^{mea}(1:1),F^{cal}(a:m)))$, and there is only one possible warping path between $F^{mea}(1:1)$ and $F^{cal}(m:m)$ with a total cost of $c(f_1^{mea},f_m^{cal})$. This validates the formula for $D(1,m)$.

Because the step size condition of the warping path is set as $p_l-p_{l-1}\in\{(0,1),(1,1),\ldots,(1,T)\}$ for $2\le l\le L$, there is no single warping path between $F^{mea}(1:n)$ and $F^{cal}(1:m)$ for $m<n$ and $1<m\le M$. This proves $D(n,m)=\infty$ for $m<n$ and $1<m\le M$.

Now, let $n\le m\le N$ and $1<m\le M$ and let $Q=(q_1,q_2,\ldots,q_L)$ be an optimal warping path for $F^{mea}(1:n)$

https://doi.org/10.1121/10.0042987

and $F^{cal}(a' : m)$. Then, the boundary conditions imply that $q_L = (n, m)$. Setting $q_{L-1} = (c, d)$, the step size condition implies $(c, d) \in \{(n, m-1), (n-1, m-1), \ldots, (n-1, m-T)\}$. Furthermore, it follows that $(q_1, q_2, \ldots, q_{L-1})$ must be an optimal warping path for $F^{mea}(1 : c)$ and $F^{cal}(a' : d)$ [otherwise, Q would not be optimal for $F^{mea}(1 : n)$ and $F^{cal}(a' : m)$]. Because $D(n, m) = c_{(q_1, q_2, \ldots, q_{L-1})}(F^{mea}(1 : c), F^{cal}(a' : d)) + c(f_n^{mean}, f_m^{cal})$, the optimality of Q implies the assertion of Eq. (20).

Theorem 1 facilitates a recursive computation of the matrix D. Upon initializing each element in D to ∞ and setting $D(1, m) = c(f_1^{mean}, f_m^{cal})$ for $m \in [1 : M]$, then, the remaining values of D are then defined recursively as in Eq. (16) for $m \leq n \leq N$ and $1 < m \leq M$. Defining the distance between the two elements $c(f_n^{mean}, f_m^{cal}) = |f_n^{mean} - f_m^{cal}|$, the algorithm for finding the optimal subsequence $F^{cal}(a^* : b^*)$ in F^{cal} to match F^{mea} and the optimal warping path is shown in Table I.

According to the algorithm shown in Table I, the reference resonance frequency sequence that is most similar to the measured resonance frequency sequence can be retrieved, and the omitted modes can be identified based on the optimal warping path.

III. RESULTS AND DISCUSSION

A. Performance of the DNN for the RUS forward problem

To form the piezoelectric sample dataset, a total of 6 40 000 digital piezoelectric samples were generated with the following randomized parameters: EPCs, clamped dielectric constants, density, and dimensions. Each material constant of a digital piezoelectric sample was scaled relative to a reference value η, with scaling factor α drawn uniformly from (0.8, 1.2). The reference values for the EPCs and clamped dielectric constants of Fuji C-213[31] are listed in Table II. The width, length, height, and density of the digital piezoelectric samples were randomly distributed within (4.512, 4.888) mm, (4.896, 5.304) mm, (4.128, 4.472) mm, and (7392, 8008) kg/m^3, respectively. The resonance frequencies of the digital piezoelectric samples were computed using the Rayleigh–Ritz method.

TABLE I. Algorithm for finding the optimal warping path.

Input: $F^{mea} = (f_1^{mea}, f_2^{mea}, \ldots, f_N^{mea})$ and $F^{cal} = (f_1^{cal}, f_2^{cal}, \ldots, f_M^{cal})$
Output: Optimal subsequence $F^{cal}(a^* : b^*)$ and warping path $P^* = (p_1, p_2, \ldots, p_L)$

Define the cumulative distance matrix $D \in \mathrm{R}^{N \times M}$ and initialize each element in D to ∞.
for $m = 1$ to M:
  $D(1, m) = |f_1^{mea} - f_m^{cal}|$.
for $n = 2$ to N:
  for $m = n$ to M:
    $D(n, m) = \min\{D(n, m-1), D(n-1, m-1), \ldots, D(n-1, m-T)\} + |f_n^{mea} - f_m^{cal}|$.
Find $b^* = \mathrm{argmin}_{b \in [1:M]} D(N, b)$.
Create a stack S to record the optimal warping path, and push (N, b^*) onto stack S.
Initialize $(n, m) = (N, b^*)$.
do
  Push $(c, d) = \underset{(s,t) \in \{(n,m-1),(n-1,m-1),\ldots,(n-1,m-T)\}}{\mathrm{argmin}} \{D(s, t)\}$ onto stack S.
  Update $(n, m) = (c, d)$.
while $m > 1$ and $n > 1$.
Pop data from the top of stack S to obtain the optimal warping path $P^* = (p_1, p_2, \ldots, p_L)$.
Obtain $p_1 = (n_1, m_1)$ and $a^* = m_1$.

A RUS forward-problem DNN comprising six layers with 256 neurons in each layer was constructed using the TensorFlow library (Google LLC, Mountain View, CA). Tanh was selected as the activation function. Batch normalization was applied to accelerate the network training.[32] The number of resonance frequencies output by the DNN was 200, that is, $M = 200$. The network parameters were trained using the digital piezoelectric samples. The batch size was 256, and the Adam optimizer[33] was used for optimization. The initial learning rate was set to 0.001; 80% of the digital piezoelectric samples were used as the training dataset, 10% as the validation dataset, and 10% as the test dataset.

The effectiveness of the DNN was assessed by calculating the relative error (RE) between the actual value, denoted as ϑ, and the estimated value, represented as ϑ^*, of the resonance frequencies

$$relative\_error(\vartheta^*, \vartheta) = \left| \frac{\vartheta^* - \vartheta}{\vartheta} \right| \times 100. \tag{21}$$

For the test samples, the REs between the resonance frequencies obtained using the Rayleigh–Ritz method and those obtained using the DNN were calculated. The mean and standard deviation of the REs attained using the DNN were 0.126% and 0.105%, respectively. The distribution of the resonance frequencies where the REs fall within various ranges is listed in Table III.

Table IV lists the first 80 resonance frequencies of a digital piezoelectric sample calculated using the Rayleigh–Ritz method and DNN. All REs were less than 0.5%.

B. Mode identification

1. Simulation study

Simulations were conducted to demonstrate the performance of the proposed automatic mode identification method. The simulation process was as follows:

Step 1: A digital piezoelectric sample was randomly selected from the piezoelectric sample dataset, and the first C resonance frequencies of the digital piezoelectric sample were used to form a resonance frequency sequence $F = (f_1, f_2, \ldots, f_C)$. Several resonance frequencies in the sequence were randomly omitted. The precise resonance frequency sequence with omitted modes is $F' = (f_1', f_2', \ldots, f_C')$, where $f_i' = -1$, if the ith mode was randomly chosen for omission; otherwise, $f_i' = f_i$ for $1 \leq i \leq C$. Then, elements with a value of -1 in F' were deleted, and the sequence became F''.

TABLE II. Reference material constants used for generating digital piezoelectric samples.

Elastic stiffness constants (10^{10} N/m^2)					Piezoelectric stress constants (C/m^2)			Dielectric constants (10^{-9} F/m)	
c_{11}^E	c_{12}^E	c_{13}^E	c_{33}^E	c_{44}^E	e_{15}	e_{31}	e_{33}	ε_{11}^S	ε_{33}^S
14.90	8.00	8.00	13.20	2.80	11.8	–5.2	17.0	7.46	7.14

Step 2: Reference digital piezoelectric samples were generated with the same clamped dielectric constants, width, length, height, and density as the selected digital piezoelectric sample selected in the step 1. For a material constant with a reference value of η, the material constant of a reference digital piezoelectric sample was $(1 + \alpha)\eta$, where $\alpha \in \{-3\delta, -\delta, \delta, 3\delta\}$ and δ is a small, fixed parameter. For the PZT sample, the number of EPCs was 8, and 65 536 (4^8) different reference digital piezoelectric samples were generated.

Step 3: The resonance frequencies of the reference digital piezoelectric samples were calculated using the RUS forward-problem DNN, and the resonance frequencies of each digital piezoelectric sample formed a reference resonance frequency sequence.

Step 4: According to the algorithm shown in Table I, the distances between the sequence F'' and the reference sequences generated in step 3 were calculated. The optimal reference resonance frequency sequence could be retrieved, and the omitted modes were identified based on the optimal warping path. Then, F'' was reordered as the identified resonance frequency sequence $F''' = (f_1''', f_2''', \ldots, f_C''')$, where $f_i''' = -1$ if the ith mode was identified for omission; otherwise, f_i''' was set to the corresponding element in F'' for $1 \le i \le C$.

Step 5: The EPCs of the piezoelectric sample were estimated using F' and F'''. The performance of the proposed automatic mode identification method was evaluated by calculating the index error (IE) between F' and F''':

$$index\_error(F', F''') = \sum_{i=1}^{C} \left(1 - \delta\left(f_i', f_i'''\right)\right)[f_i' > 0]. \quad (22)$$

The relative difference (RD) between the constant estimated using F', denoted as c', and that estimated using F''', represented as c''', is defined as

$$relative\_difference(c', c''') = \left|\frac{c' - c'''}{(c' + c''')/2}\right| \times 100. \quad (23)$$

In the simulation process, the first 100 resonance frequencies of a digital piezoelectric sample were used (i.e., $C = 100$). For each simulation, the number of omitted resonance frequencies was set to a random integer ranging from

TABLE III. Proportion of resonance frequencies corresponding to different intervals of REs between the resonance frequencies obtained using the Rayleigh–Ritz method and those obtained using the DNN.

RE (%)	Proportion of resonance frequencies
<0.05	26.41
0.05–0.1	23.14
0.1–0.2	30.43
0.2–0.5	19.30
0.5–1.0	0.71
>1.0	0.01

TABLE IV. Calculated resonance frequencies of a digital piezoelectric sample, where f and f^* correspond to resonance frequencies calculated using the Rayleigh–Ritz method and DNN, respectively.

	f (kHz)	f^* (kHz)	RE		f (kHz)	f^* (kHz)	RE
1	179.487	179.368	0.067	41	523.738	523.262	0.091
2	209.027	209.225	0.095	42	525.032	525.720	0.131
3	242.926	242.962	0.015	43	538.379	538.508	0.024
4	245.321	245.618	0.121	44	542.217	541.748	0.087
5	253.489	253.199	0.114	45	544.567	543.609	0.176
6	269.665	269.170	0.183	46	545.788	544.729	0.194
7	284.797	283.772	0.360	47	554.446	553.530	0.165
8	286.905	286.905	0.000	48	571.507	571.725	0.038
9	297.074	297.278	0.069	49	574.658	573.467	0.207
10	300.737	301.013	0.092	50	577.879	577.064	0.141
11	319.695	320.130	0.136	51	578.362	578.586	0.039
12	331.116	331.078	0.012	52	581.489	581.406	0.014
13	333.468	333.219	0.075	53	592.330	590.594	0.293
14	335.453	336.442	0.295	54	592.814	593.679	0.146
15	336.912	336.749	0.048	55	594.810	594.656	0.026
16	342.562	341.595	0.282	56	606.405	605.678	0.120
17	342.959	342.907	0.015	57	606.818	607.789	0.160
18	355.463	355.514	0.015	58	610.756	611.393	0.104
19	375.812	375.970	0.042	59	615.549	614.947	0.098
20	379.373	379.317	0.015	60	617.125	617.540	0.067
21	380.705	380.167	0.141	61	627.542	625.555	0.317
22	380.910	380.926	0.004	62	628.859	630.883	0.322
23	381.583	381.978	0.103	63	633.887	633.073	0.129
24	386.362	385.768	0.154	64	635.687	635.832	0.023
25	405.033	405.744	0.175	65	645.617	643.433	0.338
26	412.613	412.427	0.045	66	646.276	647.959	0.260
27	415.324	416.043	0.173	67	651.795	651.589	0.032
28	419.256	418.431	0.197	68	654.311	653.144	0.178
29	449.126	449.513	0.086	69	655.032	654.605	0.065
30	469.303	469.181	0.026	70	656.297	656.83	0.081
31	472.466	472.100	0.078	71	660.744	660.868	0.019
32	475.839	475.502	0.071	72	662.475	661.872	0.091
33	483.036	482.586	0.093	73	669.328	668.247	0.161
34	485.286	485.044	0.050	74	670.516	671.899	0.206
35	499.718	499.333	0.077	75	680.071	678.794	0.188
36	500.245	501.050	0.161	76	680.691	681.826	0.167
37	503.567	502.273	0.257	77	682.251	682.195	0.008
38	503.784	504.833	0.208	78	686.413	686.196	0.032
39	512.930	513.100	0.033	79	689.103	688.808	0.043
40	516.038	515.649	0.075	80	691.751	690.165	0.229

https://doi.org/10.1121/10.0042987

TABLE V. Mean RDs (%) in the EPCs of digital piezoelectric samples obtained by the RUS backward-problem DNN using precise versus identified resonance frequency sequences.

		Elastic stiffness constants (10^{10} N/m^2)					Piezoelectric stress constants (C/m^2)		
		c_{11}^E	c_{12}^E	c_{13}^E	c_{33}^E	c_{44}^E	e_{15}	e_{31}	e_{33}
δ	0.0125	0.37	0.70	0.48	0.35	0.13	0.35	1.90	0.74
	0.0375	1.24	2.10	1.59	1.19	0.46	0.79	4.95	2.51

3 to 15. We conducted 200 independent simulation experiments for each value of the parameter δ. When δ was 0.0125, the resulting mean IE was 2.98; when δ was 0.0375, the mean IE was 10.21.

To efficiently estimate the EPCs of the digital piezoelectric samples, an RUS backward-problem DNN[23] with mode omission tolerance was trained to characterize the piezoelectric samples. The RUS backward-problem DNN comprised six convolutional layers and four dense layers, where each convolutional layer had 16 filters and each dense layer had 256 neurons. The number of resonance frequencies inputted into the DNN was 90. The network parameters were trained using the digital piezoelectric samples described in Sec. III A. The EPCs of the piezoelectric samples obtained using the RUS backward-problem DNN were comparable to those obtained using the LM algorithm, while demonstrating substantially greater computational efficiency.[23]

Table V shows the mean RDs in the EPCs of the digital piezoelectric samples obtained by the RUS backward-problem DNN using the precise versus identified resonance frequency sequences. Table VI shows the mean REs between the real EPCs and those determined by the RUS backward-problem DNN using the automatically identified resonance frequencies.

2. Mode identification for the Fuji C-213 sample

The dimensions and density of the Fuji C-213 sample were $4.7087 \times 5.1495 \times 4.3117\,\text{mm}^3$ and $7772\,\text{kg/m}^3$, respectively. The resonant ultrasound spectra of the Fuji C-213 sample were measured at different temperatures using an XRUS-G10 RUS system (AcoustEvol Technology Co., Ltd., Sanya, China). The system comprises a host computer, a control and processing unit, high-temperature ultrasonic transducers (transmitter and receiver), and a transducer fixture. The host computer commands the control unit to generate a swept-frequency signal that drives the transmitted transducer. Subsequently, the mechanical vibrations of the samples are captured by the receiving transducer. Finally, the control unit processes the received signals to construct the resonant ultrasound spectra. The frequencies corresponding to the peaks in the measured resonant ultrasound spectra are the resonance frequencies. Manual mode identification was performed by matching the measured resonance frequencies with those calculated using the published EPCs.[31] Figure 2 shows the measured resonant ultrasound spectrum of the Fuji C-213 sample. Each peak in Fig. 2 represents a resonance mode; overall, 87 resonant frequencies were identified between 150 and 760 kHz and 13 modes were omitted. The inversion results for the EPCs of the Fuji C-213 sample obtained using the LM algorithm (manual mode identification) are presented in Table VI.

Reference digital piezoelectric samples were generated at different temperatures based on the published EPCs, which had the same clamped dielectric constants, width, length, height, and density as the Fuji C-213 sample. At temperature $T + \Delta T$, the characterization results obtained at T can serve as estimated values for subsequent characterization. Setting the estimated value of one material constant as η, the material constant of a reference digital piezoelectric sample was $(1 + \alpha)\eta$, and $\alpha \in \{-0.0375, -0.0125, 0.0125, 0.0375\}$. The resonance frequencies of the reference digital piezoelectric samples were calculated using the RUS forward-problem DNN, and the resonance frequencies of each digital piezoelectric sample formed the reference resonance frequency sequence.

The distances between the measured resonance frequency sequence and generated reference sequences were calculated using the algorithm shown in Table I to obtain the optimal reference resonance frequency sequence. The measured resonance frequency sequence was reordered based on the identified omitted modes. Finally, the EPCs of the Fuji C-213 sample were estimated using the RUS backward-problem DNN. Assuming that the results of manual mode identification were completely correct, the mean IE was 7.5. The EPCs characterized by RUS using the backward-problem DNN and LM algorithms at different temperatures are presented in Table VII.

The discrepancy between the material constant e_{31} characterized by RUS using the backward-problem DNN and

TABLE VI. Mean REs (%) between the real EPCs and those determined by the RUS backward-problem DNN using automatic identified resonance frequencies.

		Elastic stiffness constants (10^{10} N/m^2)					Piezoelectric stress constants (C/m^2)		
		c_{11}^E	c_{12}^E	c_{13}^E	c_{33}^E	c_{44}^E	e_{15}	e_{31}	e_{33}
δ	0.0125	0.53	0.98	0.80	0.64	0.27	0.55	3.00	1.28
	0.0375	1.30	2.22	1.75	1.33	0.52	0.88	5.66	2.71

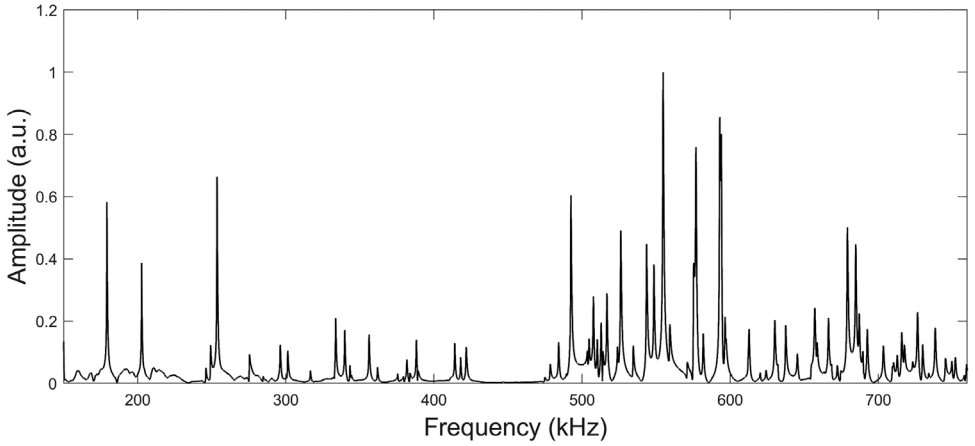

FIG. 2. Resonant ultrasound spectrum from 150 to 760 kHz at 30 °C.

LM algorithm was substantial, primarily because most modes are insensitive to the piezoelectric constant e_{31}. It should be noted that the ultrasonic resonance frequencies of rectangular parallelepiped samples of various piezoelectric ceramics, such as PZT[34] and bismuth titanate[35] are insensitive to the variation in the piezoelectric constant e31 and the dielectric constants. Moreover, RUS cannot determine the constants that weakly affect the resonance modes, such as e31 and the dielectric constants.

C. Evaluation of computational efficiency

The experiments were performed on a desktop computer with an Intel® Core™ i9-10900K CPU @ 3.70 GHz (Intel Corporation, Santa Clara, CA) and 32.0 GB RAM. To train the RUS forward-problem DNN, 6 40 000 digital piezoelectric samples were generated, and the Rayleigh–Ritz method was applied to calculate the resonance frequencies of these samples. Therefore, the calculation of the resonance frequencies must be repeated 6 40 000 times, which is time consuming. The Rayleigh–Ritz method required 6.1 s on average to calculate the resonance frequencies of a piezoelectric sample, whereas the average running time of the RUS forward-problem DNN for predicting the resonance frequencies of the piezoelectric sample was approximately 68.3 μs for mode identification.

Manual mode identification involves matching the measured resonance frequencies with the calculated reference

TABLE VII. EPCs characterized by RUS using the LM algorithm (manual mode identification) and DNN (automatic mode identification) at different temperatures.

		Elastic stiffness constants (10^{10} N/m^2)					Piezoelectric stress constants (C/m^2)		
T (°C)		c_{11}^{E}	c_{12}^{E}	c_{13}^{E}	c_{33}^{E}	c_{44}^{E}	e_{15}	e_{31}	e_{33}
20	LM	14.37	8.22	8.23	12.92	2.74	11.66	−5.72	16.22
	DNN	14.40	8.23	8.10	12.76	2.74	11.72	−5.15	16.49
	Diff[a]	0.15	0.12	1.67	1.23	0.02	0.53	10.52	1.65
30	LM	14.46	8.28	8.26	12.97	2.75	11.76	−5.65	16.41
	DNN	14.54	8.35	8.14	12.87	2.75	11.73	−5.04	16.51
	Diff	0.57	0.89	1.49	0.78	0.21	0.25	11.42	0.58
40	LM	14.48	8.28	8.27	13.00	2.76	11.85	−5.70	16.58
	DNN	14.54	8.33	8.13	12.87	2.75	11.83	−5.08	16.67
	Diff	0.45	0.65	1.73	0.95	0.21	0.14	11.45	0.54
50	LM	14.53	8.31	8.30	13.02	2.77	11.93	−5.76	16.76
	DNN	14.56	8.33	8.13	12.89	2.77	11.92	−5.10	16.84
	Diff	0.25	0.30	2.03	1.05	0.24	0.07	12.24	0.48
60	LM	14.56	8.33	8.30	13.04	2.78	12.10	−5.77	16.99
	DNN	14.48	8.21	8.09	12.82	2.79	12.15	−5.20	17.18
	Diff	0.56	1.41	2.55	1.72	0.24	0.42	10.40	1.12
70	LM	14.60	8.36	8.31	13.06	2.80	12.25	−5.77	17.27
	DNN	14.55	8.30	8.17	12.89	2.81	12.17	−5.37	17.41
	Diff	0.35	0.66	1.72	1.37	0.27	0.63	7.11	0.76

[a] $\text{Diff} = \left| \frac{c_{ij}^{E(LM)} - c_{ij}^{E(DNN)}}{\left(c_{ij}^{E(LM)} + c_{ij}^{E(DNN)}\right)/2} \right| \times 100$ or $\text{Diff} = \left| \frac{e_{ij}^{(LM)} - e_{ij}^{(DNN)}}{\left(e_{ij}^{(LM)} + e_{ij}^{(DNN)}\right)/2} \right| \times 100.$

resonance frequencies based on the estimated EPCs of the PMs, which is extremely time consuming, inherently subjective, and often leads to failed mode identification attempts. When a significant difference exists between the measured and reference resonance frequencies (indicating low similarity), it is necessary to adjust the estimated EPCs and subsequently recalculate the reference resonance frequencies. For the proposed automatic mode identification method, the average running time was approximately 36.2 s (including the time to generate 65 536 reference resonance frequency sequences).

D. Discussion

It should be noted that many DNN samples should be generated by the Rayleigh–Ritz or FEA methods using reasonable material constants. Therefore, the method presented here is only suited for mature PMs and not for new PMs whose EPCs have not been previously determined. Moreover, the DNN exhibits limited generalizability across different types of PMs. However, this does not imply that the method presented in this study is invaluable. To date, hundreds of PMs have been developed. However, only several have been commercially applied, as less than 10% of known PMs (e.g., PZT ceramics dominate >80% of the market share) have been commercially adopted. It is well known that for a specific piezoelectric ceramic or single crystal, the products provided by different producers, or even those from different batches provided by the same producer, may have exhibit material constant fluctuations. Therefore, to ensure the quality of mature PMs, producers must determine the full matrix constants of the samples from different batches. For each mature PM, such as PZT- and relaxor-based single crystals, many digital piezoelectric samples can be generated using the Rayleigh–Ritz method. Therefore, it is feasible to train specialized DNNs for each commercially relevant material. Moreover, generalizability can be enhanced by expanding the training datasets to include a wider material diversity (e.g., $BaTiO_3$ and $Bi_4Ti_3O_{12}$ ceramics) and geometric variations. After the DNN has been successfully trained, it can be repeatedly used to generate reference resonance frequency datasets for DTW automatic mode identification and to perform RUS inversion. This procedure for determining the EPCs of PMs is far more efficient than the combination of ultrasonic pulse-echo and electric resonance methods as well as the traditional RUS procedure based on manual mode identification and NLS inversion.

IV. CONCLUSION

The most challenging step in RUS is mode identification, which is the foundation for correct RUS inversion. The traditional manual mode identification method is time consuming. Therefore, the development of automatic mode identification technology is an important goal for researchers working in the field of RUS. In this study, a combination of DNN and DTW was proposed for automatic mode identification in RUS. The DNN maps the material constants to the resonance frequencies of the piezoelectric samples. After the DNN was trained successfully, it was significantly more efficient compared to that based on the Rayleigh–Ritz method. The DNN efficiently predicted the resonance frequencies of piezoelectric samples with diverse material constants. The resonance frequencies of each sample formed a reference resonance frequency sequence, and the aggregated sequences constituted a reference dataset for mode identification. A subsequent DTW algorithm was proposed to determine the optimal alignment between the measured and referenced resonance frequency sequences. This methodology identified the reference sequence that exhibited the maximal similarity to the measured sequence, thereby enabling robust mode identification.

The feasibility of using the DTW technique to conduct automatic mode identification in RUS was confirmed in this study. Automatic mode identification was performed for a Fuji C-213 PZT sample at different temperatures, and the results were comparable to those obtained manually. The automatic mode identification was significantly more efficient than manual intervention. Manual mode identification often requires more than several hours and relies strongly on the experience of the people who carry out the identification. However, the automatic mode identification system presented in this study required only tens of seconds. In this study, the resonance frequencies were manually determined from the resonant ultrasound spectra, while in future research, we will explore the automatic identification of the resonance frequencies in the spectra. This will further improve the efficiency of the RUS procedure.

ACKNOWLEDGMENTS

This work was supported by the National Natural Science Foundation of China (Grant No. 12274358); Guangdong Basic and Applied Research Foundation (Grant No. 2024A1515010019); Stable Supporting Fund of Acoustic Science and Technology Laboratory (Grant No. JCKYS2025SSJS011); and Open Fund of State Key Laboratory of Acoustics and Marine Information, Chinese Academy of Science (Grant No. SKLA202511).

AUTHOR DECLARATIONS

Conflict of Interest

The authors have no conflicts to disclose.

DATA AVAILABILITY

The data and code that support the findings of this study are available at https://osf.io/e5bvf/files/osfstorage?view_only=95fe72307f7e4d83b1e046a6bff8b4cf.

[1]A. Safari and E. K. Akdogan, *Piezoelectric and Acoustic Materials for Transducer Applications* (Springer, New York, 2008).
[2]E. Sun and W. Cao, "Relaxor-based ferroelectric single crystals: Growth, domain engineering, characterization and applications," Prog. Mater. Sci. **65**, 124–210 (2014).

[3]C. Chen, C. Huang, and Y. Chen, "Vibration analysis and measurement for piezoceramic rectangular plates in resonance," J. Sound Vib. **326**, 251–262 (2009).
[4]ANSI/IEEE Std 176-1987, *IEEE Standard on Piezoelectricity* (Institute of Electrical and Electronics Engineers, Inc., New York, 1988), Vol. 176.
[5]E. Sun, R. Zhang, F. Wu, and W. Cao, "Complete matrix properties of $[001]_c$ and $[011]_c$ poled $0.33Pb(In_{1/2}Nb_{1/2})O_3$–$0.38Pb(Mg_{1/3}Nb_{2/3})O_3$–$0.29PbTiO_3$ single crystals," J. Alloys Compd. **553**, 267–269 (2013).
[6]N. Nakamura, H. Ogi, and M. Hirao, "Elastic, anelastic, and piezoelectric coefficients of GaN," J. Appl. Phys. **111**, 013509 (2012).
[7]H. Ogi, T. Ohmori, N. Nakamura, and M. Hirao, "Elastic, anelastic, and piezoelectric coefficients of alpha-quartz determined by resonance ultrasound spectroscopy," J. Appl. Phys. **100**, 053511 (2006).
[8]R. Holland and E. P. EerNisse, "Variational evaluation of admittances of multielectroded three-dimensional piezoelectric structures," IEEE Trans. Son. Ultrason. **15**(2), 119–131 (1968).
[9]I. Ohno, "Rectangular parallellepiped resonance method for piezoelectric crystals and elastic constants of alpha-quartz," Phys. Chem. Miner. **17**, 371–378 (1990).
[10]S. Li, L. Zheng, W. Jiang, R. Sahul, V. Gopalan, and W. Cao, "Characterization of full set material constants of piezoelectric materials based on ultrasonic method and inverse impedance spectroscopy using only one sample," J. Appl. Phys. **114**, 104505 (2013).
[11]A. Migliori and J. L. Sarrao, *Resonant Ultrasound Spectroscopy* (Wiley Press, New York, 1997).
[12]L. Tang, H. Tian, Y. Zhang, and W. Cao, "Temperature dependence of dielectric, elastic, and piezoelectric constants of $[001]_c$ poled Mn-doped $0.24Pb(In_{1/2}Nb_{1/2})O_3.0.46Pb(Mg_{1/3}Nb_{2/3})O_3-0.30PbTiO_3$ single crystal," Appl. Phys. Lett. **108**, 082901 (2016).
[13]T. Lohrenz, Z. Li, and T. Fingscheidt, "Multi-encoder learning and stream fusion for transformer-based end-to-end automatic speech recognition," arXiv:2104.00120 (2021).
[14]M. Shafiq and Z. Gu, "Deep residual learning for image recognition: A survey," Appl. Sci. **12**(18), 8972 (2022).
[15]B. M. Lake, R. Salakhutdinov, and J. B. Tenenbaum, "Human-level concept learning through probabilistic program induction," Science **350**(6266), 1332–1338 (2015).
[16]L. Barbieri, E. Madeira, K. Stroeh, and W. Van der Aalst, "A natural language querying interface for process mining," J. Intell. Inf. Syst. **61**(1), 113–142 (2023).
[17]N. R. Brodnik, C. Muir, N. Tulshibagwale, J. Rossin, M. P. Echlin, C. M. Hamel, S. L. B. Kramer, T. M. Pollock, J. D. Kiser, C. Smith, and S. H. Daly, "Perspective: Machine learning in experimental solid mechanics," J. Mech. Phys. Solids **173**, 105231 (2023).
[18]B. I., K. Barashok, Y. Choi, Y. Choi, M. Aslam, and J. Lee, "Machine learning techniques in ultrasonics-based defect detection and material characterization: A comprehensive review," Adv. Mech. Eng. **17**, 1–41 (2025).
[19]O. Sabokpa, A. Zarei-Hanzaki, H. R. Abedi, and N. Haghdadi, "Artificial neural network modeling to predict the high temperature flow behavior of an AZ81 magnesium alloy," Mater. Des. **39**, 390–396 (2012).
[20]N. Haghdadi, A. Zarei-Hanzaki, A. R. Khalesian, and H. R. Abedi, "Artificial neural network modeling to predict the hot deformation behavior of an A356 aluminum alloy," Mater. Des. **49**, 386–391 (2013).
[21]Y. Zhu, W. Zeng, Y. Sun, F. Feng, and Y. Zhou, "Artificial neural network approach to predict the flow stress in the isothermal compression of as-cast TC21 titanium alloy," Comput. Mater. Sci. **50**(5), 1785–1790 (2011).
[22]W. Yang, S. Sun, J. Hu, L. Tang, L. Qin, Z. Li, and W. Luo, "Deep learning model as an inversion tool for resonant ultrasound spectroscopy of piezoelectric materials," Appl. Phys. Lett. **120**, 184101 (2022).
[23]W. Yang, S. Sun, L. Tang, W. Luo, and J. Wu, "Deep learning with mode omission tolerance as inversion tool in resonant ultrasound spectroscopy for characterizing piezoelectric materials," J. Phys. D: Appl. Phys. **58**, 305302 (2025).
[24]J. Liu, X. Zhao, K. Zhao, V. G. Goncharov, J. Delhommelle, J. Lin, and X. Guo, "A modulated fingerprint assisted machine learning method for retrieving elastic moduli from resonant ultrasound spectroscopy," Sci. Rep. **13**, 5919 (2023).
[25]H. Fukuda, A. Nagakubo, O. B. Wright, K. Kyotani, and H. Ogi, "Deep-learning-assisted resonant ultrasound spectroscopy for cubic solids," Phys. Rev. Appl. **20**, 034048 (2023).
[26]R. Wang, F. Fan, F. Shen, Y. Wang, and H. Niu, "Elastic constant estimation for low-Q materials using convolutional neural network based resonant ultrasound spectroscopy," Nondestr. Test Eval. **40**, 534–548 (2025).
[27]L. R. Rabiner and B. H. Juang, "Fundamentals of Speech Recognition," in Prentice Hall Signal Process. Ser. (1993).
[28]M. Müller, *Information Retrieval for Music and Motion* (Springer, Berlin, Germany, 2007).
[29]L. Tang, Y. Zhang, and W. Cao, "Characterizing full matrix constants of piezoelectric single crystals with strong anisotropy using two samples," J. Appl. Phys. **120**, 164102 (2016).
[30]D. E. Rumelhart, G. E. Hinton, and R. J. Williams, "Learning representations by back-propagating errors," Nature **323**, 533–536 (1986).
[31]A. Xiao, L. Tang, S. Sun, S. Wu, X. Wu, and W. Luo, "Comparison of characterization methods for assessing the temperature dependencies of elastic and piezoelectric constants of piezoelectric materials," IEEE Trans. Instrum. Meas. **72**, 6007915 (2023).
[32]C. Garbin, X. Zhu, and O. Marques, "Dropout vs. batch normalization: An empirical study of their impact to deep learning," Multimedia Tools Appl. **79**, 12777–12815 (2020).
[33]M. Reyad, A. Sarhan, and M. Arafa, "A modified Adam algorithm for deep neural network optimization," Neural Comput. Appl. **35**(23), 17095–17112 (2023).
[34]H. Li, Y. Ma, Z. Zhou, T. Yan, Y. Wu, L. Tang, S. Liu, and X. Wu, "Characterizing elastic and piezoelectric constants of piezoelectric materials from one sample using resonant ultrasound spectroscopy," J. Mater. Sci. **54**(9), 6786–6798 (2019).
[35]W. Wang, K. Zheng, S. Sun, L. Qin, L. Tang, and Z. Li, "Characterization of the full matrix constants of $Bi_4Ti_3O_{12}$ ceramics," Ceram. Int. **47**, 23518–23527 (2021).